THE JOURNAL OF PHYSICAL CHEMISTRY C

Article

pubs.acs.org/JPCC

V_{oc} from a Morphology Point of View: the Influence of Molecular Orientation on the Open Circuit Voltage of Organic Planar Heterojunction Solar Cells

Ulrich Hörmann,*[,†] Christopher Lorch,[‡] Alexander Hinderhofer,[‡,§] Alexander Gerlach,[‡] Mark Gruber,[†] Julia Kraus,[†] Benedikt Sykora,[†] Stefan Grob,[†] Theresa Linderl,[†] Andreas Wilke,[∥] Andreas Opitz,[∥] Rickard Hansson,[⊥] Ana Sofia Anselmo,[⊥] Yusuke Ozawa,[§] Yasuo Nakayama,[§] Hisao Ishii,[#,§] Norbert Koch,[∥,▽] Ellen Moons,[⊥] Frank Schreiber,[‡] and Wolfgang Brütting*[,†]

[†]Institute of Physics, University of Augsburg, Universitätsstraße 1, 86135 Augsburg, Germany

[‡]Institute of Applied Physics, University of Tübingen, Auf der Morgenstelle 10, 72076 Tübingen, Germany

[§]Graduate School of Advanced Integration Science, Chiba University, 1-33 Yayoi-cho, Inage-ku, Chiba 263-8522, Japan

[∥]Department of Physics, Humboldt University of Berlin, Brook-Taylor-Straße 15, 12489 Berlin, Germany

[⊥]Department of Engineering and Physics, Karlstad University, SE-65188 Karlstad, Sweden

[#]Center for Frontier Science, Chiba University, 1-33 Yayoi-cho, Inage-ku, Chiba 263-8522, Japan

[▽]Helmholtz-Zentrum Berlin für Materialien und Energie GmbH - BESSY II, Albert-Einstein-Straße 15, 12489 Berlin, Germany

Supporting Information

ABSTRACT: The film morphology and device performance of planar heterojunction solar cells based on the molecular donor material α-sexithiophene (6T) are investigated. Planar heterojunctions of 6T with two different acceptor molecules, the C_{60} fullerene and diindenoperylene (DIP), have been prepared. The growth temperature of the 6T bottom layer has been varied between room temperature and 100 °C for each acceptor. By means of X-ray diffraction and X-ray absorption, we show that the crystallinity and the molecular orientation of 6T is influenced by the preparation conditions and that the 6T film templates the growth of the subsequent acceptor layer. These structural changes are accompanied by changes in the characteristic parameters of the corresponding photovoltaic cells. This is most prominently observed as a shift of the open circuit voltage (V_{oc}): In the case of 6T/C_{60} heterojunctions, V_{oc} decreases from 0.4 to 0.3 V, approximately, if the growth temperature of 6T is increased from room temperature to 100 °C. By contrast, V_{oc} increases from about 1.2 V to almost 1.4 V in the case of 6T/DIP solar cells under the same conditions. We attribute these changes upon substrate heating to increased recombination in the C_{60} case while an orientation dependent intermolecular coupling seems to change the origin of the photovoltaic gap in the DIP case.

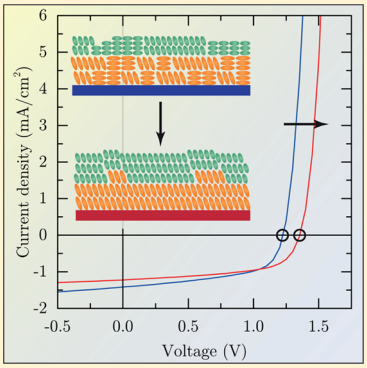

INTRODUCTION

A high open circuit voltage (V_{oc}) is one of the key factors governing the performance of a photovoltaic cell. Consequently, the origin of V_{oc} in organic donor/acceptor heterojunction solar cells has been the subject of intense research in recent years. In analogy to inorganic semiconductors, this has led to the general understanding that the open circuit voltage is vastly determined by a photovoltaic energy gap ΔE. In a broad range of material combinations this energy has been identified as the donor/acceptor intermolecular energy gap.[1−4] This is the energy difference between the highest occupied molecular orbital (HOMO) of the donor and the lowest unoccupied molecular orbital (LUMO) of the acceptor and is denoted as $E_{D/A}$ in the scope of this article. (Note that several terms exist in the literature all referring to this energy, under slightly different conditions.[1,5−9]) To determine $E_{D/A}$, it is most common to measure the HOMO levels of the donor and acceptor material separately and then derive $E_{D/A}$ by calculating the acceptor LUMO from the HOMO and the transport gap.[8] In this case it is crucial that the transport gap is precisely known and that the HOMO levels are determined in a configuration as close to the device as possible since vacuum level alignment cannot generally be assumed in an organic multilayer device.[10] In particular, intermolecular energy gaps calculated from literature values of different sources have to be treated with caution. Additionally, ΔE may be estimated by various optical[3,4,7] and electrical techniques,[3] some of which allow a more or less direct access to ΔE.[4,7] For

Received: June 21, 2014
Revised: September 30, 2014
Published: October 27, 2014

   dx.doi.org/10.1021/jp506180k | J. Phys. Chem. C 2014, 118, 26462−26470

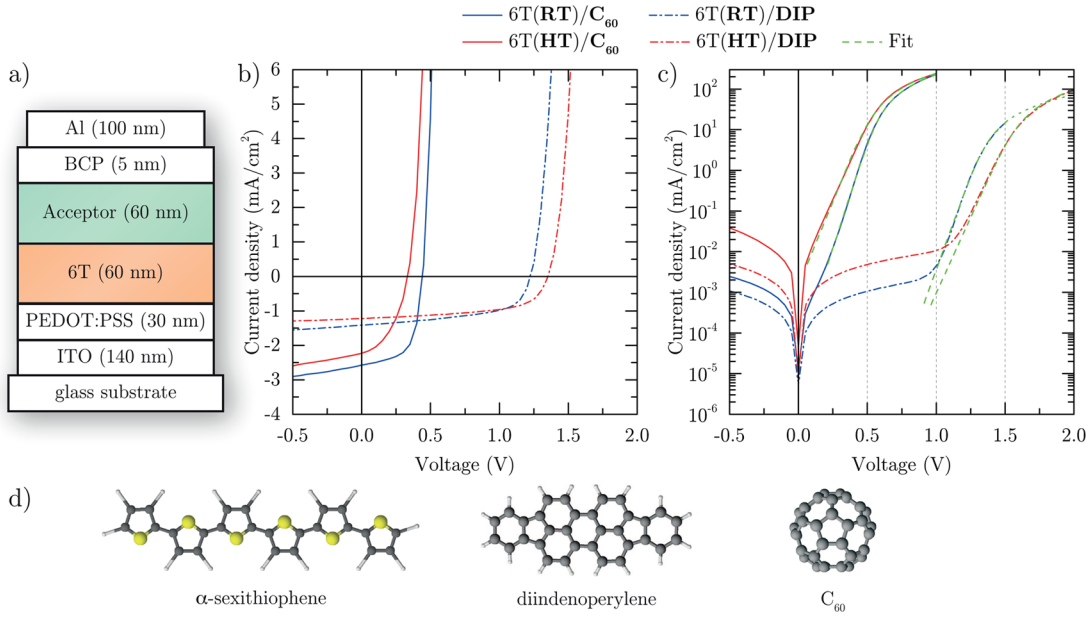

Figure 1. (a) Device stack of the investigated solar cells. Current−voltage characteristics of 6T/C_{60} (solid lines) and 6T/DIP (dash dotted lines) solar cells under illumination (b) and in the dark (c). Room temperature (RT) devices are shown in blue; devices with 6T (and only 6T) grown at a substrate temperature of 100 °C (HT), in red. The fits to the dark characteristics by the Shockley equation are shown as green dashed lines. (d) Structural formulas of the investigated materials.

example, ΔE can be extracted from the actual solar cell device by linear extrapolation of the temperature dependence of V_{oc} to 0 K.[4,7,9,11] Starting from the Shockley equation for the current−voltage (j−V) characteristics of a solar cell under illumination

$$j = j_0[\exp(eV/nk_BT) - 1] - j_{sc} \quad (1)$$

V_{oc} can be written as the voltage V measured at zero current (j = 0)

$$eV_{oc} = nk_BT \ln(j_{sc}/j_0 + 1) \quad (2)$$

Here j_{sc} denotes the short circuit current, j_0 is the reverse saturation current, n is the ideality factor, and k_B is Boltzmann's constant. By inserting the term[12]

$$j_0 = j_{00} \exp(-\Delta E/nk_BT) \quad (3)$$

we receive a relation, where V_{oc} is determined by ΔE and losses caused by recombination

$$eV_{oc} \approx \Delta E - nk_BT \ln(j_{00}/j_{sc}) \quad (4)$$

The factor j_{00} introduced in eq 3 is specific for a certain solar cell and provides a measure for the electronic coupling at the heterojunction.[6,13,14]

While ΔE sets an upper limit for the open circuit voltage at a temperature approaching 0 K, V_{oc} is commonly found to be reduced by approximately half a volt at room temperature for organic solar cells.[3,8] This can mainly be attributed to inevitable entropic losses, including radiative recombination and additional nonradiative recombination losses.[2−4,7,15−18] The magnitude of these losses strongly depends on the film morphology of the active layer. For example a larger interface area is expected to yield a larger recombination current. Thus, a planar heterojunction (PHJ) architecture is generally supposed to exhibit less recombination losses than any bulk heterojunction (BHJ) device of the same material system.[19,20] Apart from this purely geometric impact of the nanostructure, the local morphology at the donor/acceptor interface is expected to have an at least equally important impact on the recombination current: It has been shown by quantum chemical calculations that relative molecular orientation may have a strong influence on the recombination rate of a given donor/acceptor pair.[21,22] Additionally, it has recently been demonstrated that structural disorder at the donor/acceptor interface of planar heterojunctions may affect the average electronic coupling and thus the recombination rate.[23,24]

With a special focus on V_{oc} we investigate nominally planar heterojunction solar cells based on the donor α-sexithiophene (6T) and two differently shaped acceptors, the spherical buckminster fullerene C_{60} and the rod-like diindenoperylene (DIP; for structural formulas see Figure 1d).[25−27] We combine structural and energetic investigations with the analysis of solar cell device properties in order to relate the thin-film morphology to the open circuit voltage of the solar cell. The intrinsic difference in symmetry of the two acceptors yields additional insight on the effect of molecular orientation on the device characteristics.

EXPERIMENTAL SECTION

All films were prepared on indium tin oxide (ITO) covered glass slides purchased from Thin Film Devices (patterned for solar cells) and Merck (unpatterned for all other samples). In all cases the ITO substrate was spin coated with PEDOT:PSS (Heraeus Clevios AI4083) and dried in air at 150 °C for 30 min resulting in a 30 nm thick layer. 6T films were deposited by vacuum thermal evaporation (2×10^{-7} mbar) at a deposition rate of 0.3 Å/s and a substrate temperature of 100 °C or room temperature (RT), respectively. In the high temperature (HT) case, the 6T film was always cooled to room temperature in vacuum before further deposition of the acceptor layer. (Note that throughout this article RT and HT denote the growth condition of 6T and only 6T.) Subsequently C_{60} or DIP were deposited at a rate of 0.5 Å/s. Solar cell devices were transferred through a nitrogen atmosphere to a second vacuum chamber (2

dx.doi.org/10.1021/jp506180k | J. Phys. Chem. C 2014, 118, 26462−26470

Table 1. Characteristic Values and Fit Results of the Solar Cell Devices Presented in Figure 1[a]

acceptor	6T growth	j_{sc} (mA/cm^2)	V_{oc} (V)	FF (%)	PCE (%)	R_sA (Ω cm^2)	n	j_0 (mA/cm^2)
C_{60}	RT	2.6	0.44	61	0.67	1.5	1.6	3.0×10^{-5}
C_{60}	HT	2.2	0.33	43	0.31	1.5	2.1	2.2×10^{-3}
DIP	RT	1.4	1.22	57	0.97	7.5	1.8	1.7×10^{-12}
DIP	HT	1.2	1.35	59	0.96	3.4	2.3	3.4×10^{-11}

[a]The values of j_{sc}, V_{oc}, the fill factor (FF), and the power conversion efficiency (PCE) are extracted from the $j-V$ characteristics under illumination. Series resistance R_sA, ideality factor n, and dark saturation current j_0 are extracted by a fit to the dark characteristics with the Shockley equation.

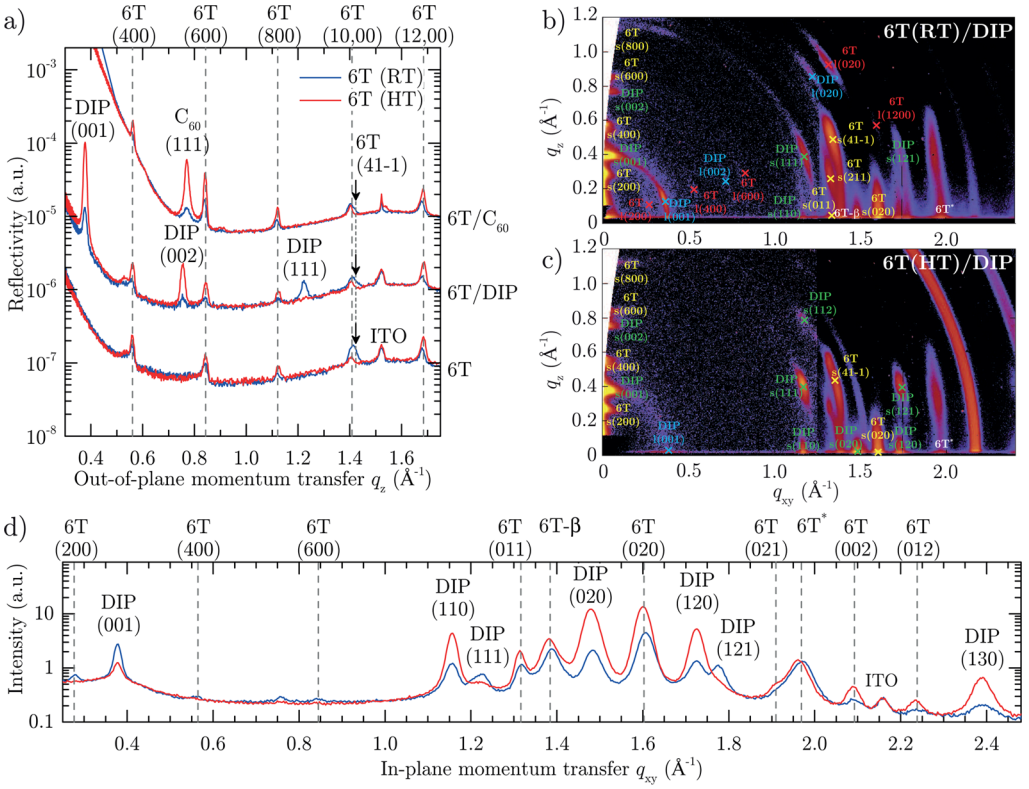

Figure 2. X-ray reflectivity spectra (a) of 6T, 6T/DIP, and 6T/C_{60} bilayers and reciprocal space maps (RT (b) and HT (c)) and GIXD sprectra (d) of 6T/DIP bilayers. Room temperature (RT) 6T films are shown in blue, and 100 °C grown 6T (HT) films are shown in red in (a) and (d). The reciprocal space maps are background corrected and stitched together from two different images. Standing 6T (DIP) is marked in yellow (green); lying 6T (DIP), in red (blue) in (b) and (c).

$\times 10^{-7}$ mbar) where bathocuproine (BCP) and aluminum were deposited to form the top contact (Figure 1a). 6T (Sigma-Aldrich), C_{60} (Creaphys), and DIP (3. Physikalisches Institut, University of Stuttgart) were purified twice by temperature gradient sublimation prior to use. BCP (Sigma-Aldrich) was used as received. X-ray reflectivity (XRR) was measured ex-situ with a GE/Seifert X-ray diffractometer (Cu Kα_1). Grazing incidence X-ray diffraction and MarCCD detector images were recorded at the ID10B (ESRF) beamline using a wavelength of 0.925 Å. Scanning force microscopy (AFM) images were recorded in air with a Thermo Microscopes Autoprobe CP-Reserach device in tapping mode. Angular resolved near edge X-ray absorption fine structure (NEXAFS) spectroscopy was performed at beamline D1011 at the MAX-lab synchrotron facility, Lund, Sweden. Using polarized monochromatic X-rays around the C 1s-edge, the total electron yield was determined by measuring the sample current. Ultraviolet photoelectron spectroscopy (UPS) measurements were performed at beamline BL8B at the Ultraviolet Synchroton Orbital Radiation (UVSOR) facility, Institute for Molecular Science (IMS), Okazaki, Japan. The photon energy, incident angle, and photoelectron emission angle were set to 30 eV, 45°, and 0° (surface normal), respectively. For valence band measurements a bias of +5 V was applied to the sample. In-situ prepared 6T layers (10 nm) for UPS measurements were deposited at a rate of 0.3−0.8 Å/s at a pressure of approximately 9×10^{-7} mbar. DIP and C_{60} layers for UPS were deposited stepwise at a rate of 0.3−0.5 Å/s in the low 10^{-5} mbar range. Current−voltage ($j-V$) characteristics were recorded with a Keithley 236 source-measurement unit. $j-V$ curves under illumination were recorded at an intensity of 100 mW/cm^2 using an LOT-Oriel solar simulator equipped with an AM1.5G filter set. Temperature dependent measurements of V_{oc} were recorded in a continuous flow liquid nitrogen cryostat (CryoVac). The solar cells were illuminated with a simulated AM1.5G spectrum at an intensity of half a sun (C_{60} samples) or roughly one sun (DIP samples).

Note that, even though characteristics of single cells are shown in this article, each is representative for the respective device type. Statistics on a minimum of five individually prepared solar cells per type (each with at least two working pixels) have shown that the presented V_{oc} values are accurate

dx.doi.org/10.1021/jp506180k | J. Phys. Chem. C 2014, 118, 26462−26470

within 20 mV (with the exception of high temperature 6T/C_{60}, which is accurate within 30 mV). A statistical error of 10−12% is estimated for the stated short circuit current values.

RESULTS

In order to get an understanding of how the film structure and the molecular orientation affect the recombination and thus the open circuit voltage in our small molecule solar cells, we start off with the electrical device characterization and then look into the morphology of the different devices by X-ray scattering, X-ray absorption, and AFM measurements. The interface energetics are studied by UPS and temperature dependent V_{oc} measurements.

Electrical Device Characterization. The device stack and the $j-V$ characteristics of PHJ solar cells of 6T/C_{60} and 6T/DIP are shown in Figure 1. The characteristic quantities are summarized in Table 1. Comparing the behavior of room temperature (blue) and high temperature (red) 6T/C_{60} cells, the curves under illumination (Figure 1b) show that V_{oc} is reduced by about 0.1 V, when 6T is grown at a substrate temperature of 100 °C. At the same time j_{sc} is decreased, which can be attributed to the drastically reduced absorption of HT grown 6T.[28] Note that, while eq 2 indicates that a reduced j_{sc} will also lead to a slightly reduced V_{oc}, the observed voltage loss is far more drastic and cannot be solely explained by the lower j_{sc}. Instead, a fit of the exponential regime of the dark $j-V$ curve (Figure 1c) with the Shockley equation (eq 1) gives deeper insight into the origin of the voltage loss. The parameters extracted from the fits are listed in Table 1. Here the dark saturation current j_0 is of special interest as it can be regarded as a measure for charge carrier recombination. In the case of HT grown 6T, j_0 is almost 2 orders of magnitude larger than in the RT case. This implies that the observed V_{oc} loss can clearly be associated with an increased recombination rate in the 6T/C_{60} device with the 6T layer grown at elevated temperature.

The dash-dotted lines in Figure 1 show the $j-V$ characteristics of 6T/DIP devices. Again a reduced j_{sc} is observed for the cell with the HT grown 6T. In contrast to the 6T/C_{60} case, despite the reduced photo current the open circuit voltage is increased by 130 mV, from 1.22 to 1.35 V, by heating the substrate during 6T deposition. The fit of the dark characteristics with the Shockley equation (dashed line in Figure 1c, parameters in Table 1) reveals that the observed difference in V_{oc} between the RT and HT devices appears not to be correlated with recombination. In particular, j_0 is about one order of magnitude larger for the high temperature grown 6T/DIP device despite its higher V_{oc}.

Structural and Morphological Investigation. The results of the X-ray reflectivity measurements are shown in Figure 2a. The spectra of both neat 6T films show peaks stemming from the (400), (600), (800), (10,00), and (12,00) lattice planes of a standing-up low temperate phase of 6T.[29] In the room temperature case (blue curve) the (10,00) peak is broadened by a contribution from the (41−1) peak, which can be assigned to flat lying 6T molecules. This phase vanishes if the film is grown at 100 °C (red curve), and only the purely upright standing phase with an angle of ∼70° between the long molecular axis and the surface is observed. Note that this is in accordance with the reduced absorption observed for HT grown 6T.[28] The optical transition dipole moment of 6T is oriented along the long molecular axis which is unfavorable for the absorption of light impinging perpendicular to the substrate.[30]

In the case of the 6T/C_{60} bilayers, C_{60} exhibits a small (111) peak of the fcc phase, when deposited onto the room temperature 6T. This peak drastically increases for C_{60} grown on top of the high temperature 6T film, indicating remarkably high crystallinity compared to the room temperature case and to what is commonly found for thin films of C_{60}.[31,32] Responsible for the intensity increase is probably also the changed orientation of the C_{60} crystallites, similar to the effects observed for C_{60} thin films on DIP.[33] The appearance of the strong C_{60} signal is accompanied by a structural change of the underlying 6T film. By comparison of the neat 6T(HT) film and the 6T(HT)/C_{60} bilayer, one can see that the fullerene seems to induce a ripening of the 6T which leads to sharper features in the XRR pattern, indicating increased crystallinity of the underlying thiophene film.

This structural change does not happen with DIP as a cover layer, where the underlying 6T appears to remain unchanged even in the high temperature case. Yet, 6T seems to have a templating effect on DIP, which grows differently on RT and HT deposited 6T. This is indicated by the DIP (111) peak visible in the X-ray reflectivity data (Figure 2a) that belongs to the flat lying λ-orientation of DIP. In films grown on 6T(RT) this phase coexists with the upright standing σ-orientation indicated by the DIP (001) and (002) peaks.[25] These peaks become far more pronounced, if DIP is grown on high temperature 6T, while the (111) peak of DIP vanishes.

Reciprocal space maps of 6T(RT)/DIP and 6T(HT)/DIP bilayers are shown in Figure 2b,c, respectively. The vanishing of lying 6T and DIP domains for HT films is clearly illustrated by the comparison of both images and confirms the results of the X-ray reflectivity measurement. Yet, a small contribution of the (100) peak of lying DIP is still visible even in the HT case. The growth of lying DIP domains has, however, previously been observed for increasing layer thickness[34,35] and is therefore expected to be present in the upper part of the film, only. This implies that only DIP in the upright standing orientation is present at the interface, when prepared on 6T films consisting of solely upright standing molecules. On the contrary, if both upright standing and flat lying domains exist in the 6T film, domains of both orientations will also coexist in the DIP layer.

The lateral coherent crystallite sizes of 6T and DIP can be extracted from the grazing incidence X-ray diffraction data shown in Figure 2d by fitting the observed peaks and applying the Scherrer equation $D = 2\pi K_s/\mathrm{fwhm}$,[36] where D is the coherent crystallite size, $K_s = 0.94$ the Scherrer factor for spherical domains, and fwhm is the full width at half-maximum of the peak. For the RT sample this yields approximate coherent crystallite sizes of 28 and 16 nm for lying and standing 6T, respectively, as well as 35 and 16 nm for lying and standing DIP. In the HT case, no lying 6T is present. The average size of crystallites of standing molecules is 18 nm for 6T and 19 nm for DIP. Crystallites of lying DIP in the upper part of the film are about 23 nm in size. Note that an additional feature denoted by 6T-β is visible in the reciprocal space maps and the grazing incidence X-ray diffraction data. This presumably stems from the β-phase of upright standing 6T molecules, previously observed in the literature.[37,38] The lateral coherent size of these crystallites is 15 nm in both cases. Unfortunately, the feature marked as 6T* cannot be clearly assigned and might be a superposition of contributions from the 6T (32−1) plane and the β-phase.

To probe the molecular orientation directly at the donor/acceptor interface, angular dependent NEXAFS spectra have

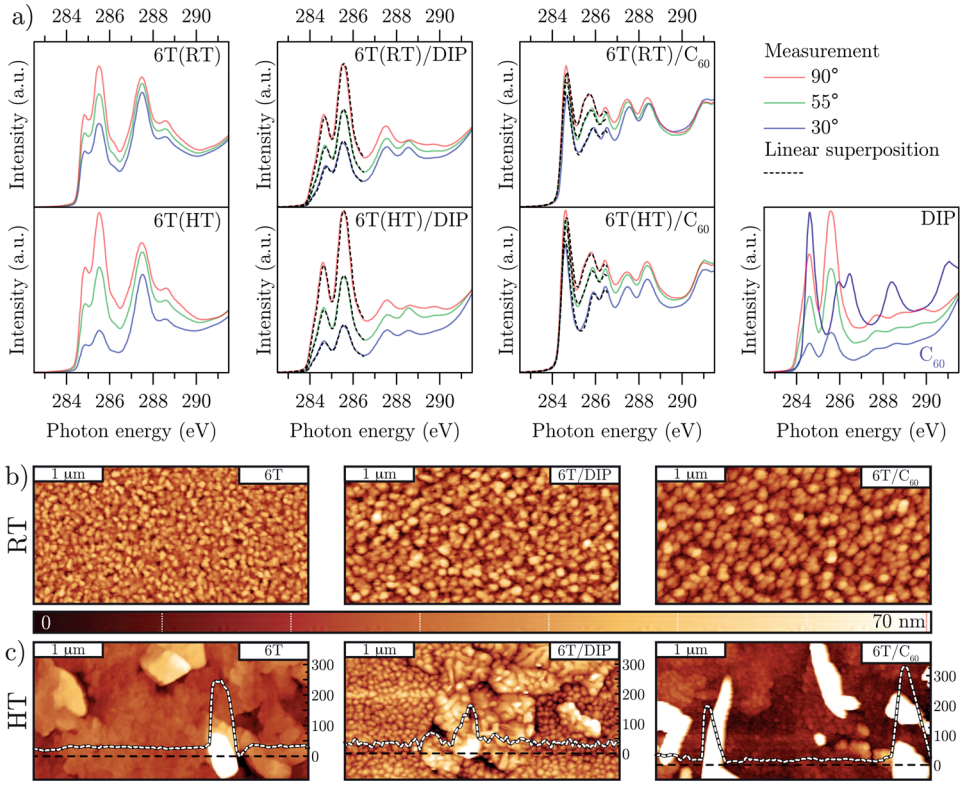

Figure 3. NEXAFS spectra for three different angles of incidence (a) and AFM images (b, c) of neat films and bilayers of 6T, DIP, and C_{60}. NEXAFS spectra of neat DIP and C_{60} (not dichroic, violet line) are shown in the right most graph in (a). Height profiles are shown as insets in the heated 6T AFM images, and the respective scale is given in nanometers at the right edge of the image. RT and HT refer to the growth conditions of the 6T film which was grown at either room temperature or at 100 °C, respectively.

been recorded for samples similar to the solar cell devices but processed on Si/PEDOT instead of ITO/PEDOT. Since NEXAFS spectroscopy is a surface sensitive technique, only thin acceptor layers of nominally 5 nm have been used in order to retain enough signal from the underlying 6T layer. Note that NEXAFS yields an average orientation angle and cannot distinguish different molecular orientations present in the probed volume. NEXAFS spectra of the investigated materials and bilayers are shown in Figure 3a. For clarity only spectra measured for 30°, 55°, and 90° angles of incidence (w.r.t the substrate plane) are shown (additionally, 40° and 70° have been measured and used for determining the angle of molecular orientation α, see the Supporting Information). The neat film spectra of RT and HT grown 6T (Figure 3a, left) show a clear dependence of the signal intensity on the angle of the incident X-rays (dichroism), where the intensities of the π^* resonances are strongest at normal incidence. This indicates that the molecules are oriented with the π^* orbitals (preferentially) parallel, and hence the conjugated plane perpendicular, to the substrate (standing molecules).[39−41] Clearly, the dichroism is stronger for the HT case compared to the RT film. This implies a larger average molecular orientation angle (more upright standing molecules) for 6T grown at an elevated temperature and is in accordance with the absence of lying 6T molecules observed by XRR. A similar trend is visible for the 6T/DIP and 6T/C_{60} bilayers. In these cases, however, the angular dependence of the NEXAFS spectrum is a superposition of that of the thin acceptor layer and a contribution from the 6T underneath. This becomes directly visible in the 6T/C_{60} spectra, where the apparent angular dependence is strongly reduced by the isotropic absorption of C_{60}. Therefore, these bilayer spectra have been deconvoluted by a best fit of the π^* region with a linear combination of the neat component spectra (neat DIP and C_{60} see far right in Figure 3a). These fits are shown as the black dashed lines in Figure 3. The relative contributions of the individual components then provide information on their respective molecular orientation.[39] The general result is in agreement with the bulk analysis presented above and confirms a mixture of lying and standing 6T at the interface for RT and only standing 6T for HT samples. Yet, 6T grown at 100 °C shows a weak tendency toward a slightly larger molecular angle at the free surface and at the interface to C_{60}, but toward a slightly smaller angle at the 6T(HT)/DIP interface compared to the bulk orientation. The same general trends are visible for RT samples but the extracted average molecular orientation angle is lower than the bulk value of standing 6T and may thus be interpreted as a superposition of contributions from standing and lying 6T molecules. Note that because of the uncertainties introduced by the deconvolution the results should be regarded as trends rather than absolute angles. Nevertheless, the differences between RT and HT are clear. For details refer to the Supporting Information.

The surface morphology corresponding to the X-ray measurements is displayed in the AFM images shown in Figure 3 (bottom). Samples with room temperature grown 6T layers are presented in Figure 3b above, and those with high temperature 6T are presented in Figure 3c under the height scale bar. All samples with 6T grown at room temperature show comparatively smooth surfaces with maximal height differences of about 70 nm at nominal thicknesses of 60 (6T) and 120 nm (6T/C_{60} and 6T/DIP). This changes drastically if 6T is grown at elevated temperatures. While a comparatively large area still

dx.doi.org/10.1021/jp506180k | J. Phys. Chem. C 2014, 118, 26462−26470

seems to be smooth, pillars as high as 250 nm (see inset in the left image of Figure 3c) appear in the neat 6T(HT) film. Simultaneously, the lateral island size increases from roughly 100 nm to about 400 nm. DIP grown on top of such a film (center image in Figure 3c) more or less preserves the present 6T topography and forms small grains on top of the 6T islands. On the other hand, if C_{60} is deposited onto a 6T film grown at 100 °C (right image of Figure 3c), the number and size of the pillars increases and small grains of C_{60} (~65 nm) are visible on top of a larger island structure that resembles the previously observed 6T structure. It seems that C_{60} induces a roughening of the 6T film.

The morphological results derived above are visually summarized in the schematics in Figure 4. Note that we

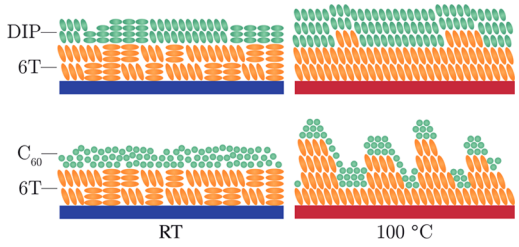

Figure 4. Schematic drawing of the morphology derived from XRD, NEXAFS, and AFM measurements. Growing 6T (orange rods) on a substrate heated to 100 °C (HT) (right) leads to an increased order of both the 6T and the acceptor top layer, which is always grown at room temperature. In the 6T(HT) case C_{60} (green spheres) induces additional crystallization and roughening of the 6T. DIP (green rods) grows purely upright standing on HT grown 6T. DIP grown on room temperature grown 6T(RT) is templated by the 6T orientation but an overgrowth of the different domains is expected.

cannot exclude that C_{60} partially "rolls" off of the large pillars and leaves fractions of the 6T uncovered. Also, it cannot clearly be distinguished between a scenario, where a roughening is caused by C_{60}, but not by DIP, and a scenario, where roughening has to be regarded as degradation of the 6T film, which is suppressed by DIP but not by C_{60}.

Interface Energetics. Even if we cannot deliberately choose the molecular orientation of 6T, we switch from a coexistence of lying and standing molecules to a standing only configuration by growing the 6T layer at an elevated temperature. This might potentially affect the interface energetics at the heterojunction.[42−44] The UPS spectra of 6T/DIP (a) and 6T/C_{60} (b) are shown in Figure 5. Films with room temperature grown 6T are shown in blue, and those with high temperature grown 6T, in red. Vertical lines mark the HOMO level onsets of the respective films. As can be seen from the energy difference ΔE_H in Figure 5a the HOMO−HOMO offsets for 6T/DIP are identical (ΔE_H = 0.75 eV), regardless of the temperature at which the 6T was grown. The same is true for 6T/C_{60} (Figure 5b) but a peculiarity occurs in this case for the HT grown 6T/C_{60} heterointerface: upon deposition of a submonolayer of C_{60} (0.3 nm) the whole spectrum, and with that the 6T HOMO onset, shifts to higher binding energies. The same shift Δ (compared to the room temperature film) is observed for the 5 nm thick bulk C_{60} film. Thus, the relative HOMO positions of 6T and C_{60} (ΔE_H = 1.65 eV) are not affected. Note that for 5 nm of C_{60} on high temperature 6T a small contribution of the underlying 6T is still present. Yet, both the baseline and the slope of the C_{60} HOMO are clearly visible; thus, the determined onset energy is

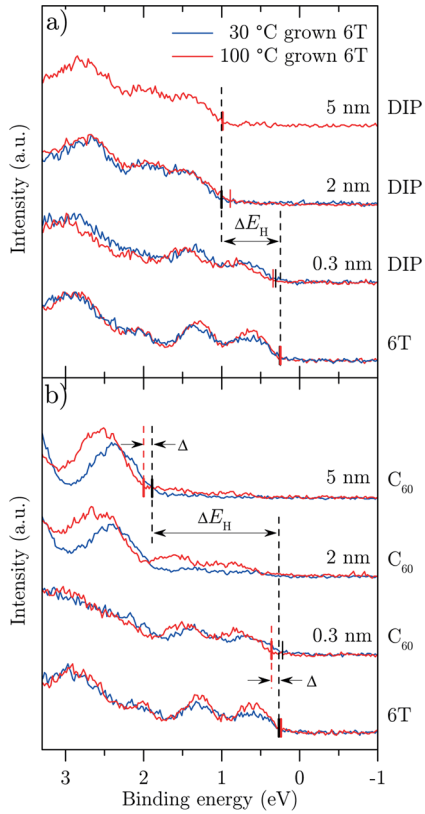

Figure 5. UPS valence region spectra of room temperature (RT) (blue) and 100 °C (HT) (red) grown 6T and DIP (a) or C_{60} (b) grown on top at room temperature. The HOMO level onsets (marked by short vertical lines) are identical within the experimental error. ΔE_H equals 0.75 eV for 6T/DIP and 1.65 eV for 6T/C_{60}.

not expected to suffer from a major impact of the 6T signal. The identical HOMO−HOMO offsets found for heated and unheated films imply that the intermolecular gaps $E_{D/A}$ remain unaffected by the growth conditions and thus by the observed morphological changes for all investigated systems.

On the other hand, in accordance with eq 4, ΔE can be extracted from electrical device characterization by measurement of the open circuit voltage for different temperatures and a linear extrapolation to 0 K.[4,7,9,11] This is shown in Figure 6 for solar cell devices prepared identically to the films presented above. Except for the RT 6T/C_{60} device, the $V_{oc}(T)$ curves show a deviation from linearity at low temperatures. This is usually accompanied by the occurrence of severely s-shaped $j-V$ curves.[45,46] For HT 6T/C_{60} this is likely due to the reduced mobility induced by the molecular orientation unfavorable for charge transport perpendicular to the substrate.[38] In the 6T/DIP case, this is expected to be caused by relatively large electron injection barriers. Both effects have a larger impact at lower temperatures.

For the 6T/C_{60} solar cells (lower data in Figure 6), both preparation conditions yield the same photovoltaic gap $\Delta E \approx$ 0.93 eV, within the uncertainty of the extrapolation although the V_{oc}'s at 300 K differ by about 100 meV (Table 1). Thus, enhanced recombination, as discussed before, seems to be the main origin for the lower V_{oc} of the HT 6T/C_{60} device. In the case of the 6T/DIP devices (upper data in Figure 6), it is clearly visible that the extracted photovoltaic gap is larger for the HT device (red triangles, 2.06 eV) than for the RT cell (blue triangles, 1.90 eV). In fact, the difference in ΔE of 160

dx.doi.org/10.1021/jp506180k | J. Phys. Chem. C 2014, 118, 26462−26470

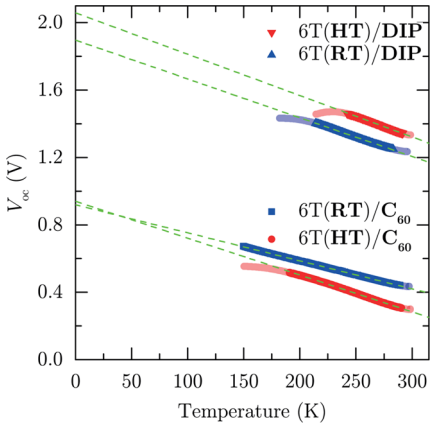

Figure 6. Temperature dependence of the open circuit voltage of 6T/C_{60} and 6T/DIP solar cells. The dashed lines represent extrapolations of the linear regimes (opaque). Blue and red data colors denote the growth condition of the respective 6T film which was at room temperature (RT) and 100 °C (HT) substrate temperature, respectively. The acceptor layer has in all cases been grown at room temperature.

meV matches well with the observed V_{oc} difference of 130 mV (Table 1) and seemingly contradicts the UPS results from which no difference of the donor/acceptor gap was concluded.

DISCUSSION

As shown above the open circuit voltage of 6T/C_{60} solar cells is strongly reduced, if 6T is grown at 100 °C substrate temperature (Figure 6). At the same time a steeper slope of the temperature dependence of V_{oc} of the high temperature device and identical gaps independent of the preparations conditions have been observed. This clearly shows that severe recombination losses at the rough 6T(HT)/C_{60} interface are indeed responsible for the observed V_{oc} loss. While it is evident that a larger interfacial area will enhance recombination, this is not likely to be the only cause of the voltage loss in this case. In fact the increase of the interfacial area estimated by AFM is well below 20%. It has been shown that the mutual molecular orientation may have a large impact on the recombination probability, too. In particular, Brédas et al. have shown by simulations that for the donor/acceptor pair pentacene/C_{60} the recombination process is far more efficient in the face-on geometry than in the edge-on configuration.[21] It seems very likely that the same is true for the 6T/C_{60} system. Just like pentacene, 6T is a rod-shaped molecule with the π-system parallel to the long molecular axis. Both configurations are expected to be present in both devices (cf. Figure 4a). The morphological investigation, however, strongly suggests that the structural disorder at the junction is significantly larger for the room temperature grown interface than for the high temperature sample. Increased disorder at the donor/acceptor interface has recently been shown to yield reduced average electronic coupling and thus larger open circuit voltages for planar squaraine/C_{60} heterojunctions and might also be responsible for the V_{oc} shift observed here.[23,24] This is strengthened by the change of the crystallite orientation in the ordered C_{60} film observed by the X-ray diffraction measurements, which also might potentially influence the donor/acceptor coupling.[21,22] Still, as was shown for pentacene and C_{60},[47] we cannot exclude additional intermixing of 6T and C_{60} at the exposed terraces in the HT device that might drastically increase the bulk heterojunction character of the HT 6T/C_{60} cell and thus significantly strengthen the role of the face-on configuration. Additionally, in such a case trap-assisted recombination would probably be significantly enhanced and might become dominant.[48,49]

By contrast, for the system of 6T and DIP an increase of the open circuit voltage is observed (Figure 6). A fit of the dark j–V characteristics suggests that this is not likely to be caused by different recombination rates. This is confirmed by the linear extrapolation of the temperature dependence of the open circuit voltage: the data yield almost identical slopes but different photovoltaic gaps (ΔE(RT) = 1.90 eV and ΔE(HT) = 2.06 eV).

In accordance with ref 8, the presented UPS data yield a donor/acceptor gap of $E_{D/A}$ = 1.8 eV for both 6T/DIP devices, if a DIP transport gap of 2.55 eV[8] is assumed. As shown in Figure 6 this is close to the ΔE value from the temperature dependent analysis of the V_{oc} for the RT sample. Surprisingly, however, it is distinctly different from the value extracted for the HT cell.

Despite the fact that a linear extrapolation of the temperature dependence of V_{oc} has been shown to yield reliable values for the intermolecular gap $E_{D/A}$ for a broad range of material systems,[9,11] it is known that this method does not result in $E_{D/A}$ under certain, extreme circumstances. Instead it has been predicted to yield the optical gap E_{opt} of the absorber, if the absorption of the charge transfer state is extremely weak, and, in particular, if the energy of the CT state comes close to the optical gap.[7,17,18,50] These special conditions seem to be fulfilled for the HT 6T/DIP device since in this case the ΔE value extracted by the extrapolation method is remarkably close to the optical gap of E_{opt} =2.1 eV of DIP.[51] This indicates that for the HT 6T/DIP device driven at typical operating temperatures the coupling between donor and acceptor molecules is too low to be relevant for the open circuit voltage. Instead, the optical gap of DIP takes the role of ΔE and seems to determine the V_{oc} for this particular solar cell.[18,52]

The identification of the photovoltaic gap ΔE with the donor/acceptor gap ($\Delta E = E_{D/A}$) for the room temperature device but with the optical gap ($\Delta E = E_{opt}$) for the high temperature cell corresponds to the morphological configurations found for the different preparation conditions: The presence of the (face-on) lying/lying 6T/DIP configuration in the RT device is expected to yield significantly enhanced electronic coupling[21,22] at the donor/acceptor interface compared to the (edge-on) standing/standing configuration prevailing in the HT morphology.

With respect to the different photovoltaic gaps ΔE identified for the two devices, the similar slopes of the linear $V_{oc}(T)$ regimes in Figure 6 indicate that the recombination losses are similar for the room temperature and the high temperature 6T/DIP cells.

Note that it is still possible to simulate the measured temperature dependences of V_{oc} of both 6T/DIP solar cells with a common donor/acceptor gap of $E_{D/A}$ = 1.8 eV from UPS and identical optical gaps of E_{opt} = 2.1 eV but with extremely different electronic coupling. The linear extrapolation then discriminates the two different energies for the two devices (see the Supporting Information).

CONCLUSION

We have investigated the impact of morphology on the open circuit voltage of organic planar heterojunction solar cells. It

dx.doi.org/10.1021/jp506180k | J. Phys. Chem. C 2014, 118, 26462–26470

was confirmed that the influence of the morphology on V_{oc} can be remarkable and that its origin is beyond simple topographical changes. For the system of 6T and C_{60}, morphology can drastically change the rate of recombination. Beyond the magnitude of the interface area this can be attributed to interfacial disorder and the mutual orientation of the donor and acceptor molecules, where the recombination rate depends on the strength of the electronic coupling.[21,23]

In the case of the 6T/DIP heterojunction two anisotropic molecules are involved. The morphological transition from a coexistence of standing and lying 6T and DIP molecules in the room temperature case to only standing molecules if 6T is grown at high temperature is accompanied by a considerable increase of the open circuit voltage. A linear extrapolation of the temperature dependent open circuit voltage suggests that different photovoltaic gaps are responsible for the observed V_{oc} difference. If, however, the well established method of determining $E_{D/A}$ by means of photoelectron spectroscopy is to be trusted, the increase of ΔE for the high temperature sample is not caused by an increased intermolecular gap. Instead, comparison with the optical gap of DIP shows that E_{opt} becomes dominant over $E_{D/A}$. This has been predicted for cases with extremely weak CT absorption[7,17,18,50,52] but to our knowledge not been reported for real devices. For these extreme conditions the interpretation of ΔE has to be reconsidered and the outcome of a linear extrapolation of $V_{oc}(T)$ toward $T = 0$ K should be taken with care.

For the room temperature 6T/DIP solar cell, the energies of the photovoltaic gap match for both methods. This is attributed to a significantly larger electronic coupling expected for the lying/lying 6T/DIP configuration than for the standing/standing orientation.

While different possible causes were proposed, combined structural and electronic simulations would help to identify the precise origin of the different electronic coupling of the four devices on a molecular level. Nevertheless, the implications of our findings are 2-fold. First, mutual orientation of donor and acceptor molecules clearly has an influence on the open circuit voltage of a solar cell. Apart from energetic changes,[53] one reason for this is orientation dependent electronic coupling.

Second, the identification of the photovoltaic gap retrieved by linear extrapolation of the open circuit voltage with the optical gap of the absorber in one case and with the intermolecular gap in another case shows that the interpretation of this method is not always straightforward and merely has to be regarded as an effective energy gap in certain cases. This might be especially true for mixtures of crystallites with different, but defined, molecular orientations.

■ ASSOCIATED CONTENT

Supporting Information

Molecular orientation from NEXAFS. Simulation of the $V_{oc}(T)$ behavior of the 6T/DIP system. This material is available free of charge via the Internet at http://pubs.acs.org.

■ AUTHOR INFORMATION

Corresponding Authors

*E-mail: ulrich.hoermann@physik.uni-augsburg.de.
*E-mail: wolfgang.bruetting@physik.uni-augsburg.de.

Notes

The authors declare no competing financial interest.

■ ACKNOWLEDGMENTS

This work was supported by the German Research Foundation (DFG) within the priority program SPP 1355 "Elementary Processes of Organic Solar Cells", by the Bavarian State Ministry of Science, Research and the Arts within the collaborative research network "Solar Technologies go Hybrid", and the Landesstiftung Baden-Württemberg. The UPS works in UVSOR were done under the Joint Studies Program [23-551] of IMS. U.H. and S.G. thank the Bavarian Research Foundation (BFS), and C.L. thanks the Carl-Zeiss-Stiftung for Ph.D. scholarships. U.H. acknowledges the Japan Society for the Promotion of Science (JSPS), and A.O. acknowledges the Röntgen-Ångström-Cluster for financial support. E.M. thanks the Göran Gustafsson Foundation for Research in Natural Sciences and Medicine. We thank Takuya Hosokai, Takeshi Watanabe and Alexei Vorobiev for helping with the X-ray measurements at the ID10B and gratefully acknowledge the technical expertise and advice of Alexei Preobrajenski, beamline manager of D1011, MAX-lab.

■ REFERENCES

(1) Rand, B.; Burk, D.; Forrest, S. Offset Energies at Organic Semiconductor Heterojunctions and their Influence on the Open-Circuit Voltage of Thin-Film Solar Cells. *Phys. Rev. B* **2007**, *75*, 115327.

(2) Scharber, M. C.; Mühlbacher, D.; Koppe, M.; Denk, P.; Waldauf, C.; Heeger, A. J.; Brabec, C. J. Design Rules for Donors in Bulk-Heterojunction Solar Cells-Towards 10% Energy-Conversion Efficiency. *Adv. Mater.* **2006**, *18*, 789−794.

(3) Veldman, D.; Meskers, S. C. J.; Janssen, R. A. J. The Energy of Charge-Transfer States in Electron Donor-Acceptor Blends: Insight into the Energy Losses in Organic Solar Cells. *Adv. Funct. Mater.* **2009**, *19*, 1939−1948.

(4) Vandewal, K.; Tvingstedt, K.; Gadisa, A.; Inganäs, O.; Manca, J. V. Relating the Open-Circuit Voltage to Interface Molecular Properties of Donor:Acceptor Bulk Heterojunction Solar Cells. *Phys. Rev. B* **2010**, *81*, 125204.

(5) Potscavage, W. J.; Sharma, A.; Kippelen, B. Critical Interfaces in Organic Solar Cells and their Influence on the Open-Circuit Voltage. *Acc. Chem. Res.* **2009**, *42*, 1758−1767.

(6) Perez, M. D.; Borek, C.; Forrest, S. R.; Thompson, M. E. Molecular and Morphological Influences on the Open Circuit Voltages of Organic Photovoltaic Devices. *J. Am. Chem. Soc.* **2009**, *131*, 9281−9286.

(7) Gruber, M.; Wagner, J.; Klein, K.; Hörmann, U.; Opitz, A.; Stutzmann, M.; Brütting, W. Thermodynamic Efficiency Limit of Molecular Donor-Acceptor Solar Cells and its Application to Diindenoperylene/C_{60}-Based Planar Heterojunction Devices. *Adv. Energy Mater.* **2012**, *2*, 1100−1108.

(8) Wilke, A.; et al. Correlation between Interface Energetics and Open Circuit Voltage in Organic Photovoltaic Cells. *Appl. Phys. Lett.* **2012**, *101*, 233301.

(9) Widmer, J.; Tietze, M.; Leo, K.; Riede, M. Open-Circuit Voltage and Effective Gap of Organic Solar Cells. *Adv. Funct. Mater.* **2013**, *23*, 5814−5821.

(10) Opitz, A.; Frisch, J.; Schlesinger, R.; Wilke, A.; Koch, N. Energy Level Alignment at Interfaces in Organic Photovoltaic Devices. *J. Electron Spectrosc. Relat. Phenom.* **2013**, *190*, 12−24.

(11) Hörmann, U.; et al. Quantification of Energy Losses in Organic Solar Cells from Temperature-Dependent Device Characteristics. *Phys. Rev. B* **2013**, *88*, 235307.

(12) Sze, S.; Ng, K. K. *Physics of Semiconductor Devices*, 3rd ed.; Wiley Interscience: Hoboken, NJ, 2007; p 95.

(13) Yamamoto, S.; Orimo, A.; Ohkita, H.; Benten, H.; Ito, S. Molecular Understanding of the Open-Circuit Voltage of Polymer:-Fullerene Solar Cells. *Adv. Energy Mater.* **2012**, *2*, 229−237.

(14) Schlenker, C. W.; Thompson, M. E. The Molecular Nature of Photovoltage Losses in Organic Solar Cells. *Chem. Commun.* **2011**, *47*, 3702−3716.
(15) Rau, U. Reciprocity Relation between Photovoltaic Quantum Efficiency and Electroluminescent Emission of Solar Cells. *Phys. Rev. B* **2007**, *76*, 085303.
(16) Kirchartz, T.; Taretto, K.; Rau, U. Efficiency Limits of Organic Bulk Heterojunction Solar Cells. *J. Phys. Chem. C* **2009**, *113*, 17958−17966.
(17) Giebink, N. C.; Wiederrecht, G. P.; Wasielewski, M. R.; Forrest, S. R. Thermodynamic Efficiency Limit of Excitonic Solar Cells. *Phys. Rev. B* **2011**, *83*, 195326.
(18) Koster, L. J. A.; Shaheen, S. E.; Hummelen, J. C. Pathways to a New Efficiency Regime for Organic Solar Cells. *Adv. Energy Mater.* **2012**, *2*, 1246−1253.
(19) Ray, B.; Lundstrom, M. S.; Alam, M. A. Can Morphology Tailoring Improve the Open Circuit Voltage of Organic Solar Cells? *Appl. Phys. Lett.* **2012**, *100*, 013307.
(20) Hinderhofer, A.; Schreiber, F. Organic-Organic Heterostructures: Concepts and Applications. *ChemPhysChem* **2012**, *13*, 628−643.
(21) Yi, Y.; Coropceanu, V.; Brédas, J.-L. Exciton-Dissociation and Charge-Recombination Processes in Pentacene/C_{60} solar cells: Theoretical Insight into the Impact of Interface Geometry. *J. Am. Chem. Soc.* **2009**, *131*, 15777−15783.
(22) Yi, Y.; Coropceanu, V.; Brédas, J.-L. A Comparative Theoretical Study of Exciton-Dissociation and Charge-Recombination Processes in Oligothiophene/Fullerene and Oligothiophene/Perylenediimide Complexes for Organic Solar Cells. *J. Mater. Chem.* **2011**, *21*, 1479−1486.
(23) Fu, Y.-T.; da Silva Filho, D. A.; Sini, G.; Asiri, A. M.; Aziz, S. G.; Risko, C.; Brédas, J.-L. Structure and Disorder in Squaraine-C_{60} Organic Solar Cells: A Theoretical Description of Molecular Packing and Electronic Coupling at the Donor-Acceptor Interface. *Adv. Funct. Mater.* **2014**, *24*, 3790−3798.
(24) Zimmerman, J. D.; Xiao, X.; Renshaw, C. K.; Wang, S.; Diev, V. V.; Thompson, M. E.; Forrest, S. R. Independent Control of Bulk and Interfacial Morphologies of Small Molecular Weight Organic Heterojunction Solar Cells. *Nano Lett.* **2012**, *12*, 4366−4371.
(25) Dürr, A. C.; Schreiber, F.; Münch, M.; Karl, N.; Krause, B.; Kruppa, V.; Dosch, H. High Structural Order in Thin Films of the Organic Semiconductor Diindenoperylene. *Appl. Phys. Lett.* **2002**, *81*, 2276−2278.
(26) Horlet, M.; Kraus, M.; Brütting, W.; Opitz, A. Diindenoperylene as Ambipolar Semiconductor: Influence of Electrode Materials and Mobility Asymmetry in Organic Field-Effect Transistors. *Appl. Phys. Lett.* **2011**, *98*, 233304.
(27) Banerjee, R.; Novák, J.; Frank, C.; Lorch, C.; Hinderhofer, A.; Gerlach, A.; Schreiber, F. Evidence for Kinetically Limited Thickness Dependent Phase Separation in Organic Thin Film Blends. *Phys. Rev. Lett.* **2013**, *110*, 185506.
(28) Hörmann, U.; Wagner, J.; Gruber, M.; Opitz, A.; Brütting, W. Approaching the Ultimate Open Circuit Voltage in Thiophene Based Single Junction Solar Cells by Applying Diindenoperylene as Acceptor. *Phys. Status Solidi, Rapid Res. Lett.* **2011**, *5*, 241−243.
(29) Horowitz, G.; Bachet, B.; Yassar, A.; Lang, P.; Demanze, F.; Fave, J.-L.; Garnier, F. Growth and Characterization of Sexithiophene Single Crystals. *Chem. Mater.* **1995**, *7*, 1337−1341.
(30) Yassar, A.; Horowitz, G.; Valat, P.; Wintgens, V.; Hmyene, M.; Deloffre, F.; Srivastava, P.; Lang, P.; Garnier, F.; Gamier, F. Exciton Coupling Effects in the Absorption and Photoluminescence of Sexithiophene Derivatives. *J. Phys. Chem.* **1995**, *99*, 9155−9159.
(31) Wagner, J.; et al. High Fill Factor and Open Circuit Voltage in Organic Photovoltaic Cells with Diindenoperylene as Donor Material. *Adv. Funct. Mater.* **2010**, *20*, 4295−4303.
(32) Opitz, A.; Wagner, J.; Brütting, W.; Hinderhofer, A.; Schreiber, F. Molecular Semiconductor Blends: Microstructure, Charge Carrier Transport, and Application in Photovoltaic Cells. *Phys. Status Solidi* **2009**, *2694*, 2683−2694.
(33) Hinderhofer, A.; Gerlach, A.; Broch, K.; Hosokai, T.; Yonezawa, K.; Kato, K.; Kera, S.; Ueno, N.; Schreiber, F. Geometric and Electronic Structure of Templated C_{60} on Diindenoperylene Thin Films. *J. Phys. Chem. C* **2013**, *117*, 1053−1058.
(34) Dürr, A.; et al. Interplay Between Morphology, Structure, and Electronic Properties at Diindenoperylene-Gold Interfaces. *Phys. Rev. B* **2003**, *68*, 115428.
(35) Kowarik, S.; Gerlach, A.; Sellner, S.; Schreiber, F.; Cavalcanti, L.; Konovalov, O. Real-Time Observation of Structural and Orientational Transitions during Growth of Organic Thin Films. *Phys. Rev. Lett.* **2006**, *96*, 125504.
(36) Scherrer, P. Bestimmung der Grösse und der inneren Struktur von Kolloidteilchen mittels Röntgenstrahlen. *Nachr. Ges. Wiss. Goettingen, Math. Kl.* **1918**, *1918*, 98−100.
(37) Moser, A.; et al. A Disordered Layered Phase in Thin Films of Sexithiophene. *Chem. Phys. Lett.* **2013**, *574*, 51−55.
(38) Servet, B.; et al. Polymorphism and Charge Transport in Vacuum-Evaporated Sexithiophene Films. *Chem. Mater.* **1994**, 1809−1815.
(39) Stöhr, J.; Outka, D. A. Determination of Molecular Orientations on Surfaces from the Angular Dependence of Near-Edge X-Ray-Absorption Fine-Structure Spectra. *Phys. Rev. B* **1987**, *36*, 7891−7905.
(40) Koller, G.; Berkebile, S.; Krenn, J. R.; Netzer, F. P.; Oehzelt, M.; Haber, T.; Resel, R.; Ramsey, M. G. Heteroepitaxy of Organic-Organic Nanostructures. *Nano Lett.* **2006**, *6*, 1207−1212.
(41) Sitter, H.; Resel, R.; Koller, G.; Ramsey, M.; Andreev, A.; Teichert, C. In *Organic Nanostructures Next Generation Devices*; Al-Shamery, K., Rubahn, H.-G., Sitter, H., Eds.; Springer: Berlin, 2008; pp 3−19.
(42) Duhm, S.; Heimel, G.; Salzmann, I.; Glowatzki, H.; Johnson, R. L.; Vollmer, A.; Rabe, J. P.; Koch, N. Orientation-Dependent Ionization Energies and Interface Dipoles in Ordered Molecular Assemblies. *Nat. Mater.* **2008**, *7*, 326−332.
(43) Huang, Y. L.; Chen, W.; Huang, H.; Qi, D. C.; Chen, S.; Gao, X. Y.; Pflaum, J.; Wee, A. T. S. Ultrathin Films of Diindenoperylene on Graphite and SiO_2. *J. Phys. Chem. C* **2009**, *113*, 9251−9255.
(44) Han, W. N.; et al. Quantitatively Identical Orientation-Dependent Ionization Energy and Electron Affinity of Diindenoperylene. *Appl. Phys. Lett.* **2013**, *103*, 253301.
(45) Kraus, J. K. Physics of Molecular Donor-Acceptor Solar Cells. Ph.D. Thesis; University of Augsburg, 2013.
(46) Wagner, J.; et al. Identification of Different Origins for s-Shaped Current Voltage Characteristics in Planar Heterojunction Organic Solar Cells. *J. Appl. Phys.* **2012**, *111*, 054509.
(47) Fu, Y.-T.; Risko, C.; Brédas, J.-L. Intermixing at the Pentacene-Fullerene Bilayer Interface: A Molecular Dynamics Study. *Adv. Mater.* **2013**, *25*, 878−882.
(48) Nalwa, K. S.; Kodali, H. K.; Ganapathysubramanian, B.; Chaudhary, S. Dependence of Recombination Mechanisms and Strength on Processing Conditions in Polymer Solar Cells. *Appl. Phys. Lett.* **2011**, *99*, 263301.
(49) Foertig, A.; Wagenpfahl, A.; Gerbich, T.; Cheyns, D.; Dyakonov, V.; Deibel, C. Nongeminate Recombination in Planar and Bulk Heterojunction Organic Solar Cells. *Adv. Energy Mater.* **2012**, *2*, 1483−1489.
(50) Faist, M. A.; Kirchartz, T.; Gong, W.; Ashraf, R. S.; McCulloch, I.; de Mello, J. C.; Ekins-Daukes, N. J.; Bradley, D. D. C.; Nelson, J. Competition Between the Charge Transfer State and the Singlet States of Donor or Acceptor Limiting the Efficiency in Polymer:Fullerene Solar Cells. *J. Am. Chem. Soc.* **2012**, *134*, 685−692.
(51) Heinemeyer, U.; et al. Exciton-Phonon Coupling in Diindenoperylene Thin Films. *Phys. Rev. B* **2008**, *78*, 085210.
(52) Nelson, J.; Kirkpatrick, J.; Ravirajan, P. Factors Limiting the Efficiency of Molecular Photovoltaic Devices. *Phys. Rev. B* **2004**, *69*, 035337.
(53) Graham, K. R.; et al. Re-Evaluating the Role of Sterics and Electronic Coupling in Determining the Open-Circuit Voltage of Organic Solar Cells. *Adv. Mater.* **2013**, *25*, 6076−6082.